Development of ductile polymer composites with designable interfacial adhesion

OTKA FK 124352

final report

01/12/2017 – 31/05/2022

1. Introduction, aims of the project

In the previous decades of composite research, the main aim was to create composite systems with extreme load-bearing capacity. Therefore, researchers and companies focused on the production of strong fibers and a maximal fiber-matrix adhesion for sufficient load transfer to the matrix. The achievement of this goal helped composites to reach a significant market share in safety-critical sectors as transportation, energy, and construction. Most of the structures which were replaced by composite ones were metal structures, where besides the high strength, ductile behavior was also present, providing a level of safety. While (especially carbon fiber reinforced) composites could even surpass metals in terms of strength, their failure behavior is brittle. In common cases, after reaching their stress maximum at a relatively low deformation, a catastrophic failure occurs. This is quite unpleasant in safety-critical applications. To overcome this problem, researchers around the globe are focusing on the creation of pseudo-ductile composites by different methods, modifying the matrix (filling with rubber particles, lower level of curing, etc.) or the reinforcement (slight misorientation, hybridization, cutting, etc.). In our research, we aimed to achieve pseudo-ductility by the modification of the third "component" of the composite system: the interface between the fibers and the matrix by several techniques, introducing some advantages through the clever design of the modification by creating different patterns at the interface. Our initial research goals were:

- development of different interlaminar patterning technologies based on 3D printing, LASER micro structuring, and spraying of an interphase modifier material,
- thoroughly investigate the effect of the designed interlaminar properties and the mechanisms leading to higher ductility, reaching a deep understanding of the connection between interfacial adhesion and composite ductility,
- investigate the possibility and effectiveness of healing provided by the patterned interface through the crack filling and crack tip blunting effect of the melted interphase modifier material.

In the following chapters, we try to comprehensively summarize the results of our 4.5 years-long research project.

2. Investigation of interfacial adhesion modification methods

Based on our preliminary experiments, we have decided to focus on the following interfacial adhesion modification methods:

- FFF (Fused Filament Fabrication) 3D printing of interfacial materials, which is compatible with the matrix, creating an interlaminar pattern, which shows lower adhesion to the matrix material
- LASER treatment of the reinforcing fibers, ablation of the sizing material, therefore creating patterns with zones where the lack of sizing provides the lower interfacial adhesion
- Chemical removal of sizing material, which provides lower adhesion zones

2.1. 3D printed interlaminar patterns

Polycaprolactone (PCL) was selected as the material for the creation of the 3D printed interlaminar patterns, preliminary experiments were also performed with PESU (Polyether Sulfone), but these were not as successful as PCL. Firstly the effect of adding PCL to the epoxy matrix was investigated. Therefore we have created different mixtures of EP/PCL. For the whole line of our experiments, we have used IPOX MR 1010 DGEBA-based epoxy resin (a widely used high-performance epoxy resin type) with IPOX MH 3124 room temperature hardener (standard amine-based curing agent), or IPOX MH 3111 high-temperature hardener (high-temperature hardener, which gives unlimited room temperature pot life, and provides excellent glass transition temperature after curing), ESUN eMorph175N05 PCL filament and Zoltek PX35FBUD0300 unidirectional carbon weave. To investigate the effect of adding PCL to the EP matrix, DMA tests (TA Q800, 5 Hz, 2°C/min, 3 point bending setup) were performed on the EP/PCL specimens with different compositions.

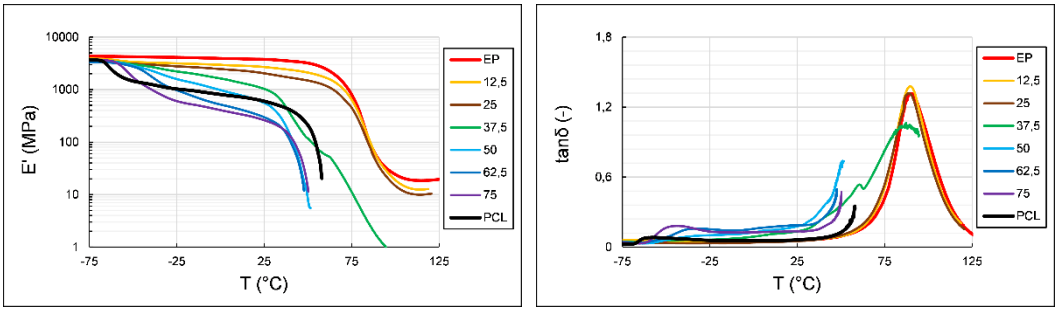

Figure 1. DMA curves of the EP/PCL specimens (numbers in the legend represent PCL content in %)

From the curves presented in Figure 1, it can be seen that as the concentration of PCL m/m% increases, the value of E' starts to decrease significantly at lower temperatures, which is close to the temperature of the T_m of PCL. Rubbery plateau no longer occurs for mixtures containing as little as 50m/m%, which may indicate phase inversion. The rubbery plateau observed in the ranges below 50m/m% PCL may indicate that a continuous EP phase is still present in these samples. The reason for the decrease in the rubbery plateau is that the density of crosslinks decreases with increasing PCL concentration, more PCL chains may be looped between the crosslinks, and in addition, in this temperature range, the PCL was already present in a sediment state, which increased the segmental movements significantly. The distinct maximum peak at tanδ values indicates good mixing, and its decrease may also indicate a decrease in crosslink density, which at higher concentrations (above 50m/m%) has already fallen below the peak of pure PCL. From the curves, it can be observed that the T_g temperature characteristic of PCL increases

with decreasing additive concentration. The transition temperature also appears on the mixtures, even for the mixture containing 12.5 m/m% PCL, the peak appeared shifted. The shift can be explained by the fact that the epoxy T_g transition temperature is higher than that of PCL, towards which this transition temperature of the mixture is shifted. From the peak that appears, it can be concluded that PCL forms a continuous phase in the system. Based on our results, we have assumed that probably an interpenetrating network (IPN) was generated from the two polymers. To confirm this at the micro-level, we have performed atomic force microscopy (AFM, Nanosurf Flex-AFM) investigations, looking for the fine-grained phase separation characteristic for IPN systems. The AFM images are presented in Figure 2.

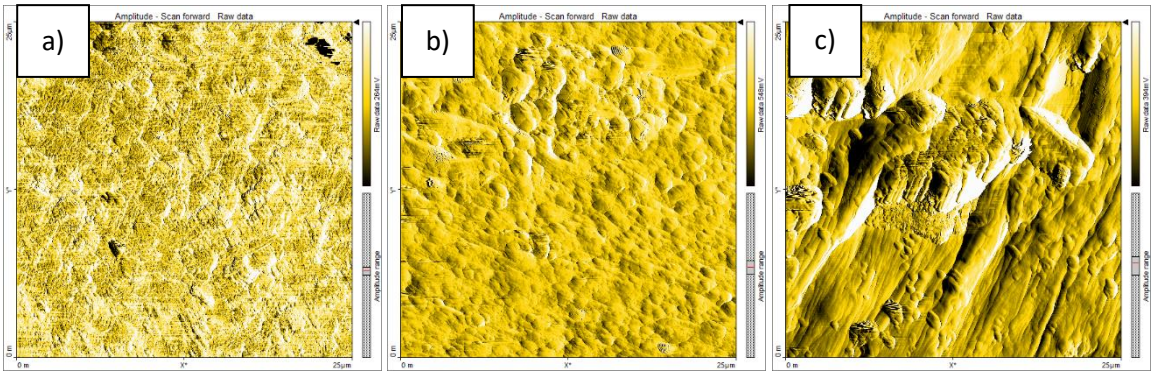

Figure 2. AFM images of the a) 25 weight%, b) 50 weight%, c) 70 weight% PCL containing EP/PCL specimens

The images of Figure 2 show the phase separation typical of IPN systems. The lighter parts show the lower attenuation zones typical of epoxy resin, while the darker parts show the higher attenuation zones typical of PCL. For the 25m/m% sample, the role of the matrix is taken by the epoxy system, but already at 50/m% phase inversion appears with PCL taking over the role of the embedding matrix. Furthermore, at 75m/m% it is observed that the epoxy material forms larger islands, creating a less dispersed system. By definition, the system also belongs to a special subgroup within IPN materials since IPN systems appear mainly in crosslinked materials. Thus, in the case of the PCL-Epoxy resin blend, it can be considered as a partial (semi-)IPN system. Classically, we speak of such systems in the case of entanglement of two crosslinked systems, but it can also occur between linear and crosslinked systems. The decreas in the T_g of the epoxy in the DMA studies can be explained by the fact that the distance between the bonds of the crosslinked system increases with increasing PCL concentration. The penetrating PCL stretches the segments between the bonding points, or even at some point hinders their formation. To illustrate this phenomenon, we have created Figure 3.

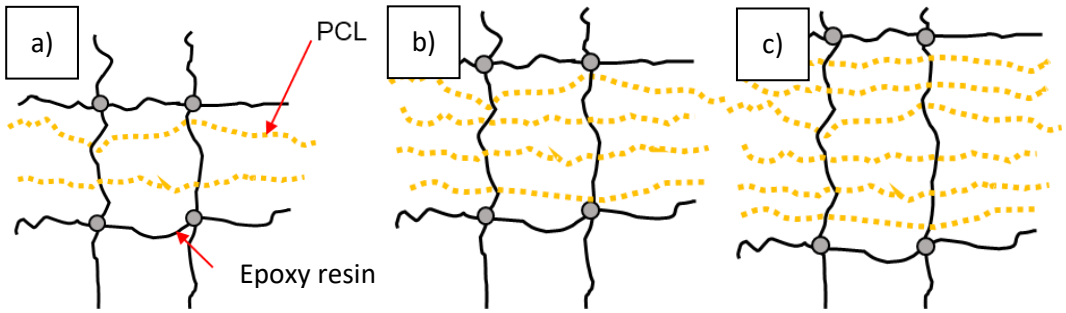

Figure 3. Schematic illustration of the formation of the semi-IPN system in a) 25 weight%, b) 50 weight%, c) 70 weight% PCL containing EP/PCL specimens

After investigating the structure of the EP/PCL system, we have focused on the investigation of the fiber-matrix interfacial adhesion change caused by the local introduction of PCL to the resin. Therefore we performed microdroplet tests (Zwick Z005, 20 N load cell, 2 mm/min, 30 µm blade distance, geometry measurement with Olympus BX51M) on CF/EP(/PCL) specimens with different compositions of the EP/PCL microdroplets (Figure 4).

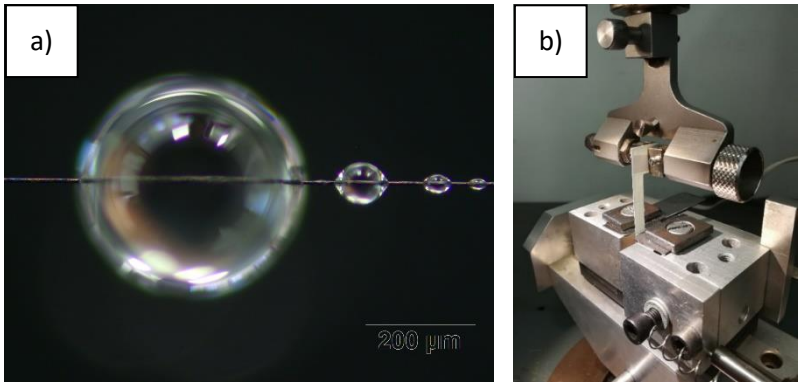

Figure 4. EP/PCL microdroplet on a single carbon fiber (a), setup of the microdroplet tests (b)

The results of the microdroplet tests, the calculated interfacial shear strength values are presented in Figure 5 in the function of PCL content of the microdroplet.

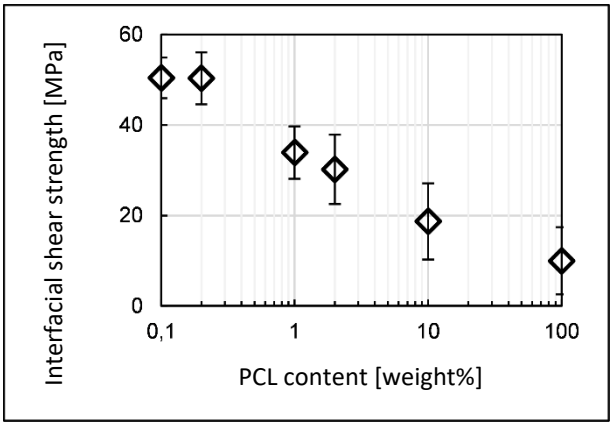

Figure 5. Results of the microdroplet tests

It can be said that with increasing the concentration of PCL, the shear strength decreases significantly compared to the reference samples. It can be said that for the composite samples, the PCL is present at 100% concentration at the interface so that the significant change in adhesion occurs there. Due to the reduced interfacial shear strength, the load transfer can be varied locally, so that zones can be created locally that can modify crack propagation. The reduction is already significant at concentrations as low as 1 m/m%. Already in this case, PCL phases appeared at the interface, which significantly weakened the matrix-fiber interface.

To prove the effectiveness of the creation of designed semi-IPN zones in achieving pseudo-ductility four types of interlaminar patterned specimens were created, the zone layouts are presented in Figure 6, the structure of the composites is presented in Figure 7.

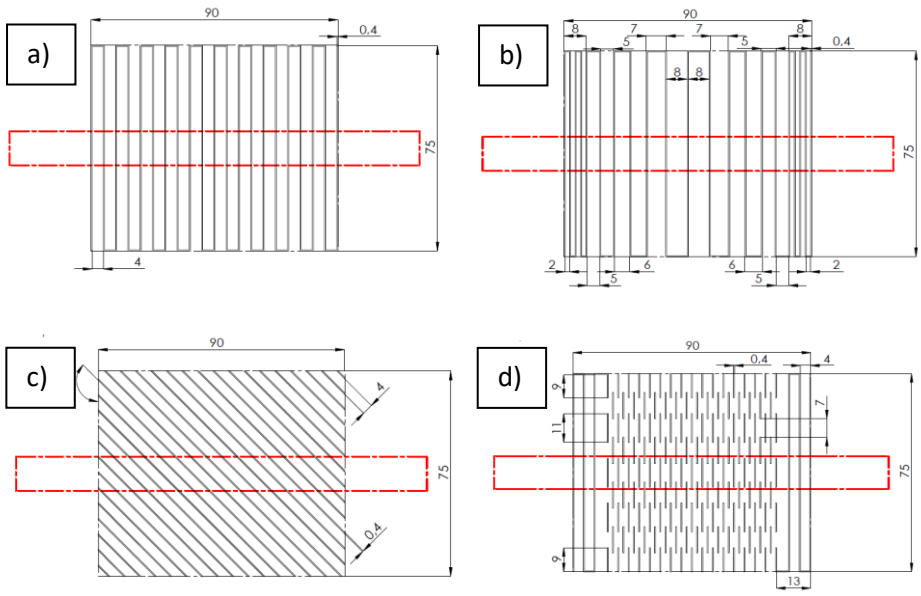

Figure 6. Interlaminar patterned zone layouts, a) Parallel; b) Edge-effect; c) Diagonal; d) Combined (red area represents the specimen orientation)

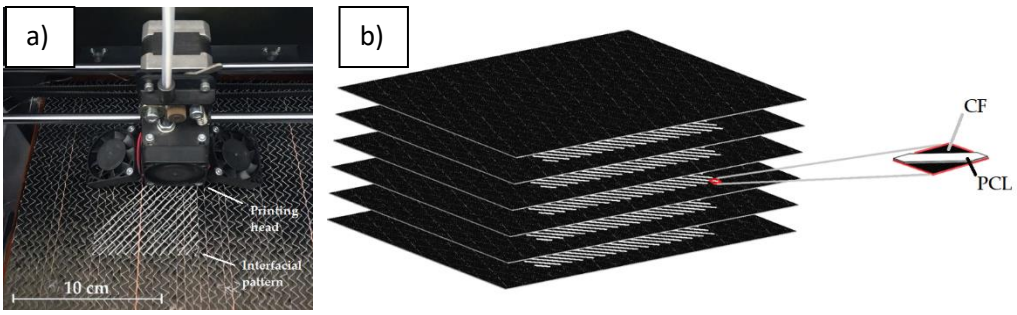

Figure 7. Creation of the interfacial pattern on carbon weave (a), exploded view of the composite laminate, five interlayers with printed diagonal zones and the desired macrostructure (b)

We have performed tensile, three-point bending, and Charpy impact tests on the specimens. The most prominent effect was present in the case of the flexural and Charpy impact properties. The curves recorded during the bending tests are presented in Figure 8.

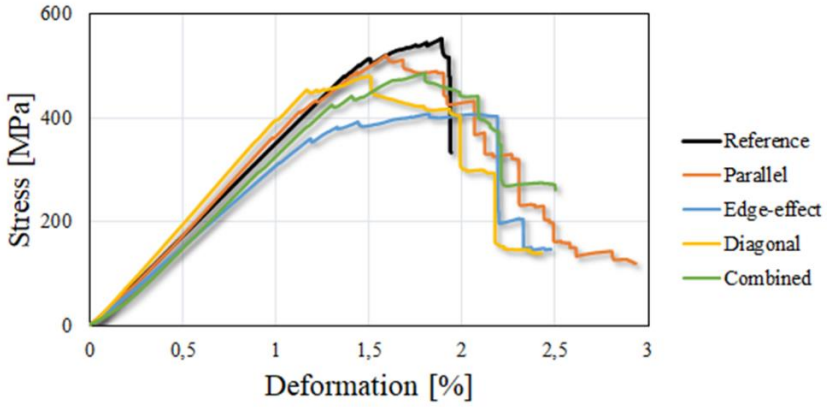

Figure 8. Three-point bending test curves of the interlaminar patterned samples with different patterns

There is one prominent difference between the strength values (Figure 8) of the specimens: a 100 MPa fall in the maximal bending stress of the edge-effect grid. The other modified samples behaved in nearly the same way as the reference samples. The maximum stress is also reached earlier by the modified samples, but with a longer ductile plateau; the final failure is reached at much higher deformation. The different behaviors can be attributed to the different designs of the grids. In the case of the edge-effect grid, there is a significant decrease in strength. The reason for this can be that the adhesion rate is significantly reduced at two points locally. Therefore, the cracks can be concentrated at these points. The different grids enhance ductility to different degrees; the diagonal and combined grid has several distinct weakened adhesion regions, which makes cracks more likely to collide with these zones.

In the case of the reference specimens, after the maximum stress (σ_m) was reached, the specimens did not show any resistance; they broke suddenly. In the case of the modified samples, after this limit was reached, failure was prolonged, and deformation at the maximal stress (ε_m) also increased. To determine damage progress, we investigated the bending curves around the maximal stress (Figure 8). There are many steps before maximal stress is reached in the case of the reference specimens, which indicates a higher energy release during failure at each step. Failure happens with significant drops in the stress level with high energy release. Therefore, these specimens cannot take considerable deformation after reaching maximum stress (Table 1). In the case of the modified samples, the curve is much flatter, which indicates damage at several local points. The specimens with a modified grid were significantly more deformable; final failure appeared at higher deformation (ε_b). The area under the curve shows the specific absorbed energy (SAE) during the bending test. In the case of modified samples, the absorbed energy increased significantly.

	E [GPa]	σm [MPa]	εm [%]	σb [MPa]	εb [%]	SAE[MJ/m3]	DI [-]
Reference	36.8±3.6	556.7±27.0	1.8±0.2	340.2±101.0	2.0±0.1	6.7±0.3	0.81±0.13
Parallel	36.0±2.5	529.4±28.6	1.8±0.2	304.4± 90.4	2.3±0.1	7.3±0.3	0.72±0.14
Edge-effect	32.0±2.7	405.6±17.4	1.7±0.3	267.0±135.1	2.6±0.2	7.1±0.3	0.65±0.15
Diagonal	35.9±4.1	465.4±39.2	1.5±0.2	233.2±136.3	2.4±0.1	7.7±0.3	0.54±0.11
Combined	30.6±3.7	451.6±44.1	1.6±0.2	167.8± 62.4	2.6±0.4	7.3±0.4	0.66±0.14

Table 1. Results of the three-point bending tests

In the case of the tensile tests, the most prominent results were the thermocamera images, which showed a very severe heat concentration in the case of the reference sample, paired with a catastrophic failure (Figure 9, left), and much more homogeneous heat distribution in the case of interface-modified samples (Figure 9, right).

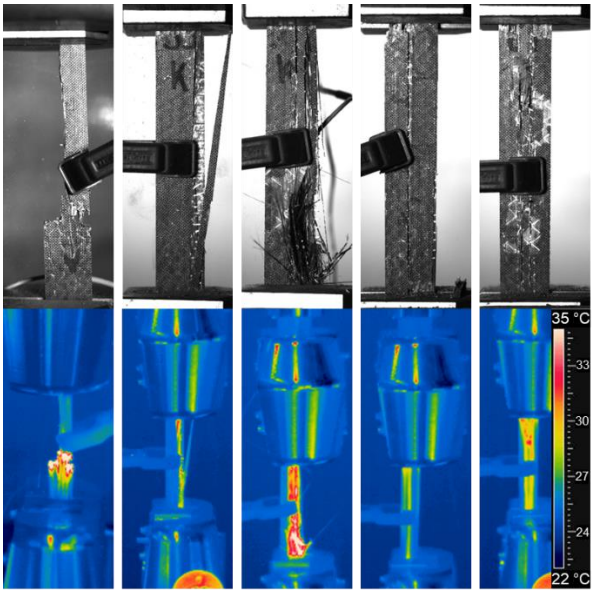

Figure 9. Photographs (top) and thermocamera images (bottom) of reference (first to the left) and interfacially modified samples (right)

The pseudo-ductile behavior can also be observed in stress-time curves the instrumented Charpy impact specimens (Figure 10).

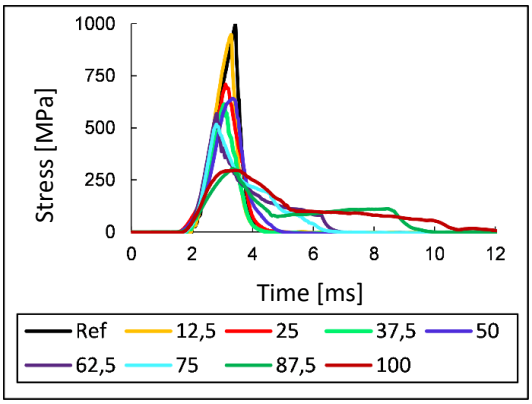

Figure 10. Instrumented Charpy impact curves of the reference and interfacially modified samples (numbers in legend correspond to PCL content in the matrix in %)

In the case of the Charpy impact tests, not only pseudo-ductility was observed, but also an interesting other phenomenon occurred. The fracture surface generated corresponded well to the contour of the interlaminar pattern, the failure position could be preselected with the help of interfacial patterning (Figure 11). This can serve as a starting point for a new research direction.

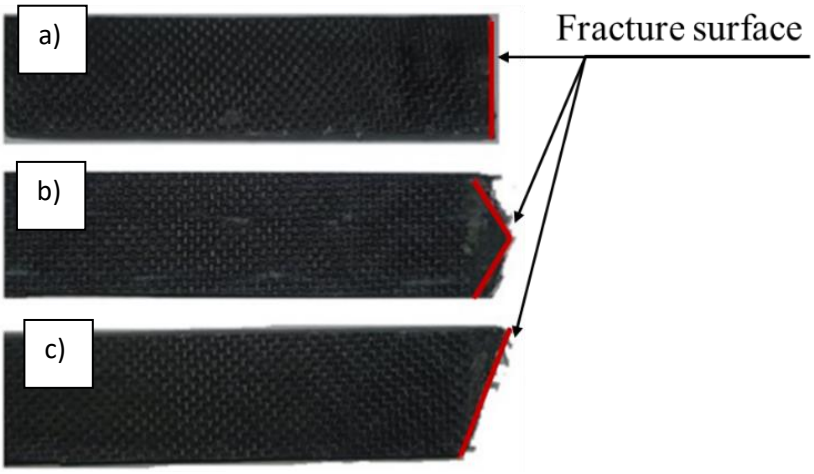

Figure 11. Broken Charpy impact specimens: reference (a), biaxial/diagonal chessboard pattern (b), diagonal pattern (c)

These results proved the effectiveness of FFF 3D printing interlaminar patterning to achieve pseudo-ductility. From the tested methods, this proved to be the most effective and reproducible, to it was selected for the further investigation of the effect of interlaminar patterning on the pseudo-ductility of composites.

2.2. LASER patterned interface

A second tested option of interfacial patterning was to use LASER to ablate the sizing of the reinforcement in designed locations. By this method, no new material is added to the system, but the coupling agent is removed from the interface, causing weakened adhesion. To create the interlaminar pattern, a VersaLaser VLS 2.30 CO_2 LASER was used. In the case of the LASER engraver, two main technological parameters could be set, the power in a 0 to 100% range and the feed speed. If the pattern

is created by setting a lower speed, the dwell time at each location, so the energy input is increased, this causes the removal of more material, firstly the removal of the sizing, but after that the damage of the fibers. The results of some treatments with different parameters are presented in Figure 12.

Figure 12. LASER treated carbon UD weave

Based on the first results, the introduced energy was controlled by the number of passes of the LASER beam and not the fine-tuning of the speed, providing a more controlled heat input. The parameters tested are presented in Table 2.

Case number	LASER power [%]	Speed [%]	Number of passes [-]
1	10-100	50	1
2	10-100	50	2
3	10-100	100	1
4	10-100	100	2

Table 2. Tested parameters of LASER patterning

The effect of the LASER treatment was evaluated firstly through SEM images. Above 70% LASER power and 50% speed, severe degradation of the fibers could be observed with damaged and broken fibers. The samples were also investigated with SEM (Figure 13).

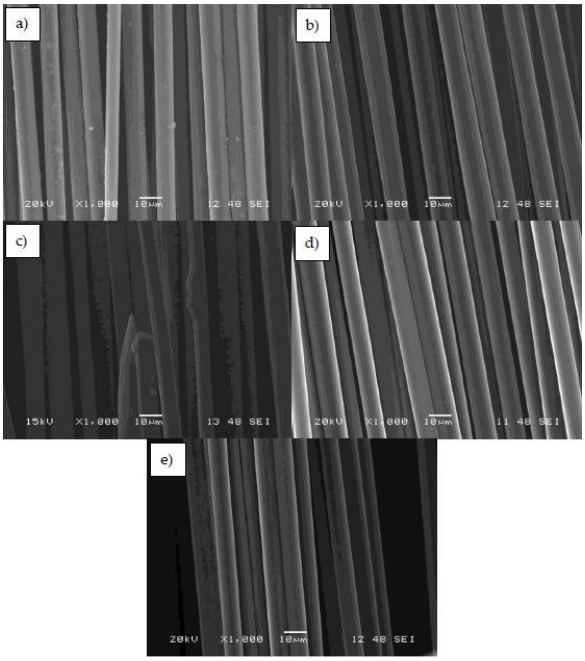

Figure 13. Carbon fiber samples without (a) and after LASER treatment (100% power, b – case number 1, c – case number 2, d – case number 3, e – case number 4)

For the treatments, it can be said that for sample 2 the fibers degraded at maximum power. For the other samples, no significant changes were observed compared to the untreated reference sample, only impurities were removed. Presumably, the sizing stood more or less intact, as the smooth surface was retained for samples 1, 3, and 4, which is typical of surface-sized fibers. This was different for sample 2. In the next step, we investigated for which power level a suitable surface treatment occurs first without significant degradation of the fibers. This occurred at 40% power, 50% speed, and two passes. This parameter set was used for the creation of the tested diagonal pattern (see Figure 6c), which was engraved on the surface of the carbon weaves at different surface fill ratios (0, 33, 67, and 100%).

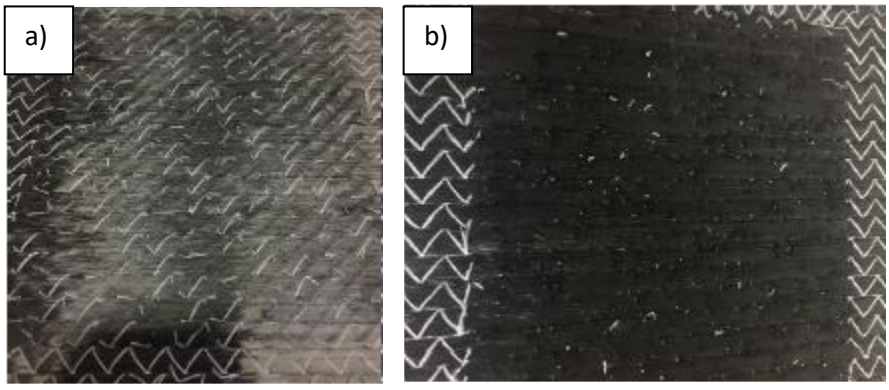

Figure 14. Carbon fiber samples with a 33% (a) and 100% (b) surface filled diagonal LASER engraved pattern

The same set of testing was performed on the samples as in the case of the 3D printed versions. The stress-deformation curves of the three-point bending tests are presented in Figure 15.

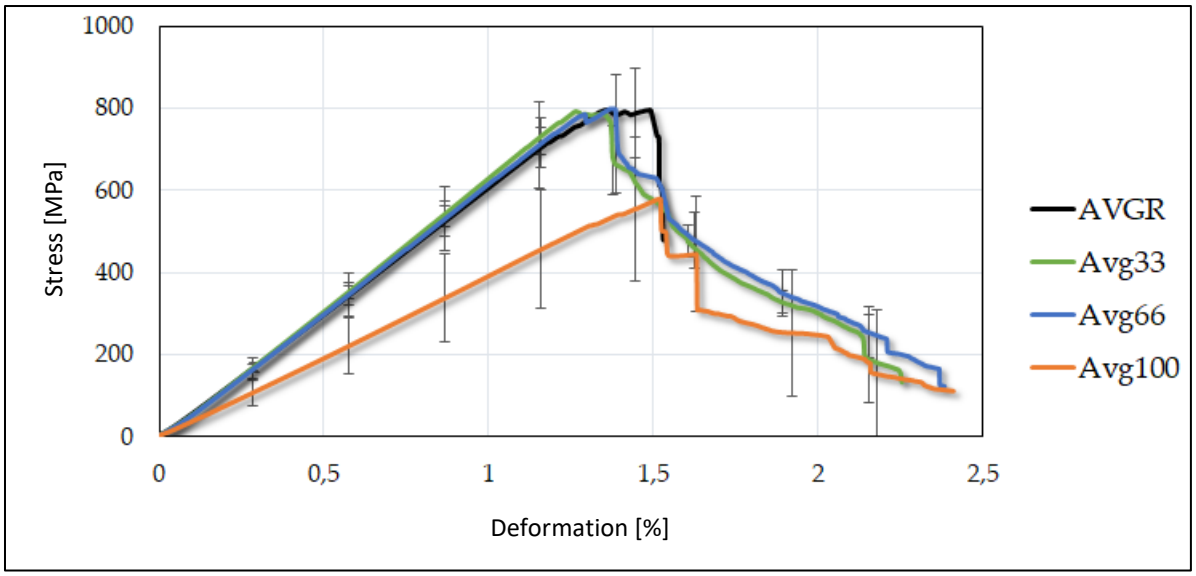

Figure 15. Average stress – deformation curves of the three-point bending tests of the LASER engrave interface samples

It can be seen that with the removal of the sizing by the LASER treatment, a gradual failure appeared after the maximum load was reached. It can be said that, as in the case of the technology based on sizing removal, the mechanical properties of the system deteriorated significantly at complete surface fill. This is due, in this case, to the fact that the composite could no longer fully perform its function. The load could not be transferred properly from the matrix to the reinforcement at the complete treated length. This may also be the reason for the wider scatter band, which is also reflected in the mechanical properties in the case of higher surface treatments. In the case of the lower fill ratios, the pseudo-ductile plateau emerged without a significant loss in maximum stress.

Similar results were observed in the case of the Charpy impact tests. An approximately 20% decrease in ductility index (so an increase in ductility) could be measured, with an approximately 10% loss of impact energy.

As a conclusion, it can be declared, that the pseudo-ductile behavior could be also achieved by the LASER treatment, but the results were inferior to the results of the FFF technology.

2.3. Chemical surface modification

A third tested option of interfacial patterning was to chemically remove the sizing from the fibers according to a given pattern. Firstly to find the right solvent, the sizing material type had to be identified by FTIR measurement. According to the measurement, the sizing is based on DGEBA epoxy. For removing the sizing chromic acid (H2CrO4) was used. For the creation of the interlaminar pattern, a mask had to be created from polypropylene (PP), resembling the desired pattern geometry. The mask was produced from a thin PP foil by LASER cutting. After placing the foil on the reinforcing CF layer, the chromic acid was sprayed on the mask, so it could only contact the sizing at the cutout resembling the pattern (Figure 16).

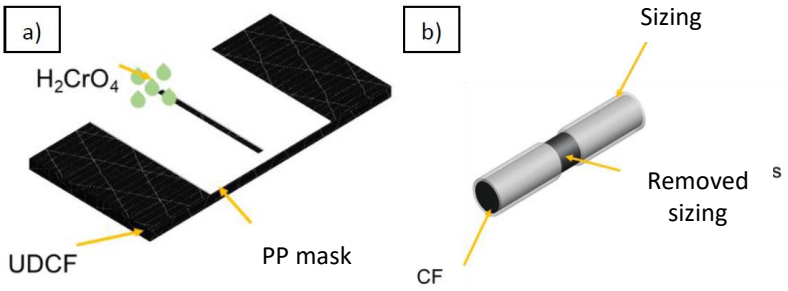

Figure 16. Schematic representation of the creation of the interfacial pattern by H2CrO4 solvent (a) local image of treated fiber (b)

To check the effectiveness, microdroplet tests were performed with the same parameters which were used for the FFF technology in Chapter 2.1. The results are presented in Figure 17.

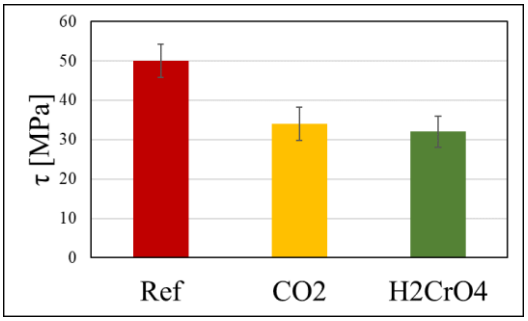

Figure 17. Results of the microdroplet tests of the untreated (Ref), LASER treated (CO2), and acid treated (H2CrO4) carbon fibers with epoxy matrix

When comparing the results to the ones obtained by 3D printing, we can clearly make a difference. While in the case of the 3D printed patterns, still there are some covalent bonds available, in the case of the LASER treated and acid-treated samples, the adhesion is physical. With the 3D printing technique, lower interfacial shear strength values can be reached, due to the very low adhesion of the PCL to the epoxy sizing. The results proved that the adhesion modification was achieved, so again, the diagonal patterned samples were produced as in 2.1 and 2.2 for the sake of comparison. Three-point bending tests were performed on the composites to compare the performance of the three adhesion modification techniques. Characteristic average stress-deformation curves are presented in Figure 18.

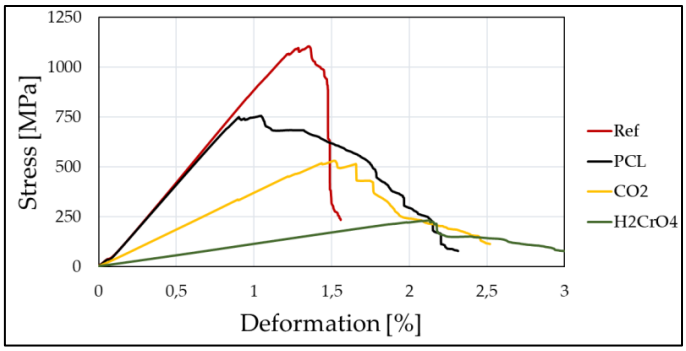

Figure 18. Average thee point bending curves of the untreated (Ref), FFF patterned (PCL), LASER patterned (CO2), and acid patterned (H2CrO4) interface carbon fiber reinforced epoxy composites

From the results, the three technologies can be clearly compared. While in all cases, the pseudo-ductility occurred, the price in strength was way too high in the case of the LASER treatment and in the case of the acid treatment. Based on this, the 3D printing technology was chosen for the further investigation of the possibilities of interlaminar patterning.

3. Investigation of the effects of interlaminar patterning and the mechanisms behind it

To investigate the effect of the interlaminar patterns on the pseudo-ductile behavior of modified composites three-point bending, tensile, Charpy impact, and ENF (end-notched flexure tests were carried out). For each test, diagonal chessboard patterned samples were prepared. The average three-point bending test result curves are presented in Figure 19.

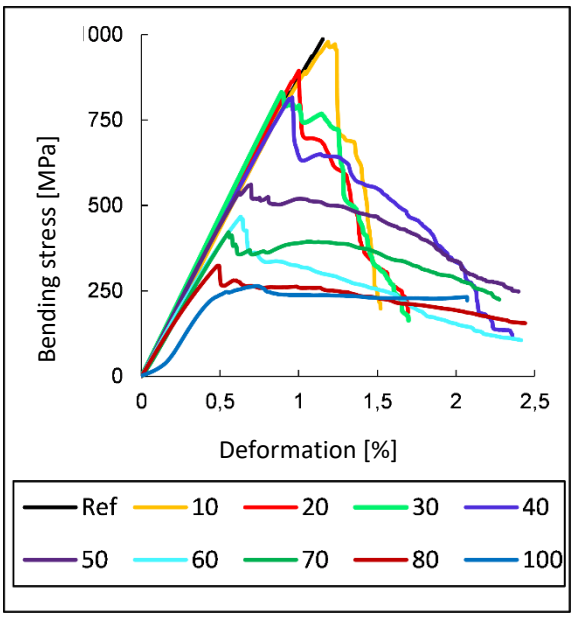

Figure 19. Average thee point bending curves of the interfacially modified samples (numbers in the legend represent PCL contents in %)

For the reference specimens, once the flexural strength was reached, no further deformation was possible, with the appearance of brittle failure. In comparison, the modified specimens were able to

withstand further loading with significant further sub-strain. As a result, the modified specimens exhibited tough, plastic-like damage. To further check the effect of the interfacial pattern parameters, samples with fixed line thickness, fixed number of zones were created with biaxial patterns besides the biaxial (diagonal chessboard) patterned samples. The concept for the creation of the different patterns is presented in Figure 20.

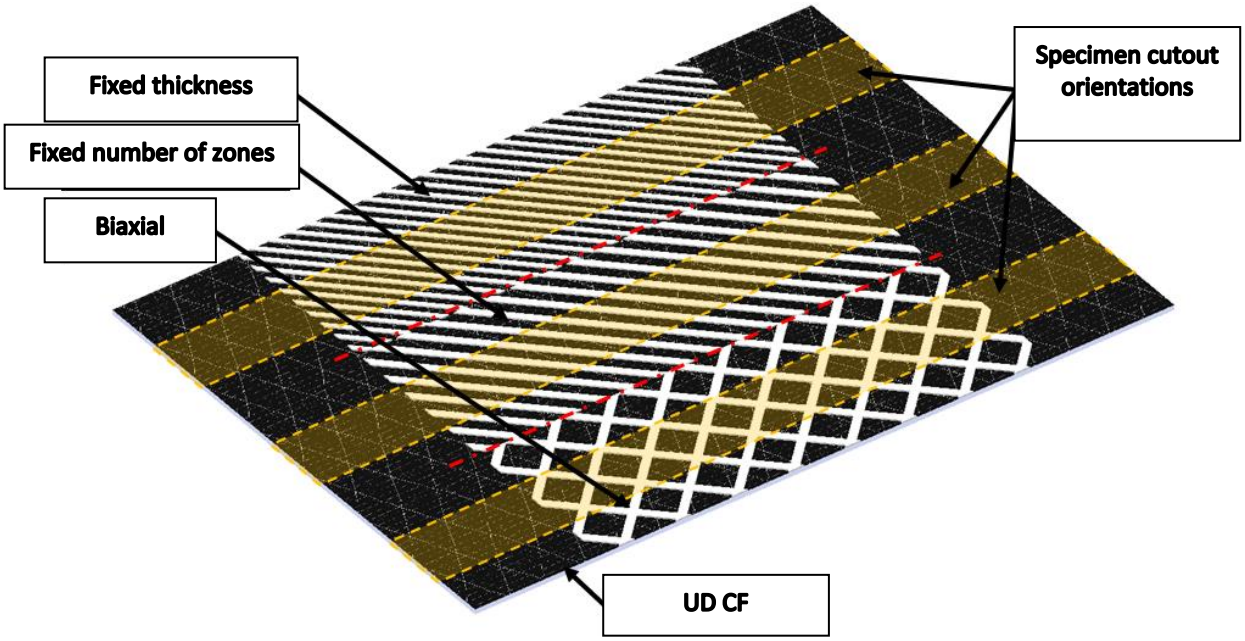

Figure 20. The concept for the creation of the interfacial patterns

Results of the three-point bending tests are presented in Figure 21.

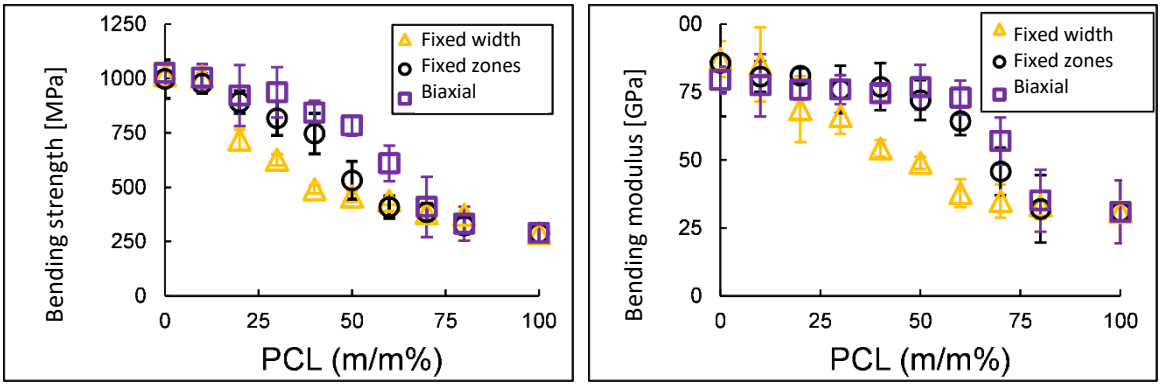

Figure 21. Results of the three-point bending tests

By observing the bending strength values, it can be seen that a continuous decrease occurred with increasing PCL content. This trend is also observed in the flexural modulus values. There is no difference between the patterns, but the rate of change is different. This may be due to the fact that the spacing between the elements decreases faster for the fixed thickness designs compared to the other designs. This is important in crosslinking occurs, because the distance between PCL zones is smaller than in other designs, i.e. the distance between the treated zones is smaller during melting. During

melting, this distance is filled sooner, i.e. the near 100m/m% PCL interlayer material content appears sooner. Furthermore, considering the flexural modulus and strength values, it is observed that the composites approach the properties of the 100m/m% PCL-CF composite.

The observed saturation effect at the strength and modulus values can be well approximated by logistic equations. The variable parameter used in the studies was the amount of thermoplastic material, it's effect can be investigated on the strength and modulus of the system. For this purpose, it is useful to choose a function that also describes such a change. Based on the increase in dose, several approximations have been investigated, which may be suitable for a proper approximation of the measured points. Finally, we have chosen the Hill equation used in biochemistry, whose analogy is well suited to characterize the response to an increase in the dose of the thermoplastic substance (1),

$$Y = A \cdot \left(\frac{(100-S)^n}{K_{0,5}^n + (100-S)^n} \right) \quad (1)$$

where "Y" is the reaction rate, "A" is the maximum reaction rate, "S" is the solution concentration, "K0,5" is the half reaction rate, and n is the Hill coefficient. Basically, the parameters of the equation need to be interpreted for the application. In the case of a composite system, "A" can be understood as a proportionality factor that depends on the maximum values of the system, if the values are between 0 and 1, the value of "A" will take be one. The concentration term "S", for the composite system, depends on the mass concentration of the PCL, the degree of dosage of which is proportional to the term. The Hill coefficient can be broken down into three values. In biochemistry, it gives the cooperative tendency between the solution and the enzymes. If n > 1, the coefficient describes a positive interaction, i.e. the enzymes can bind more easily to the molecules of the solution. In the case of equality, the enzymes can bind to the solvent molecules in the same number as the number of solvent molecules in the system. "K0,5" gives the apparent binding propensity in the equation. Based on studies of different saturations, its value gives the location of the inflection point on the curves as a function of concentration.

By examining the system (Figure 22), it can be observed that the decreasing trend occurs earlier for the fixed width design compared to the other designs. The reason for this can be found in the merging of the zones, which will be discussed later. The values of the Hill equations are presented in Table 2.

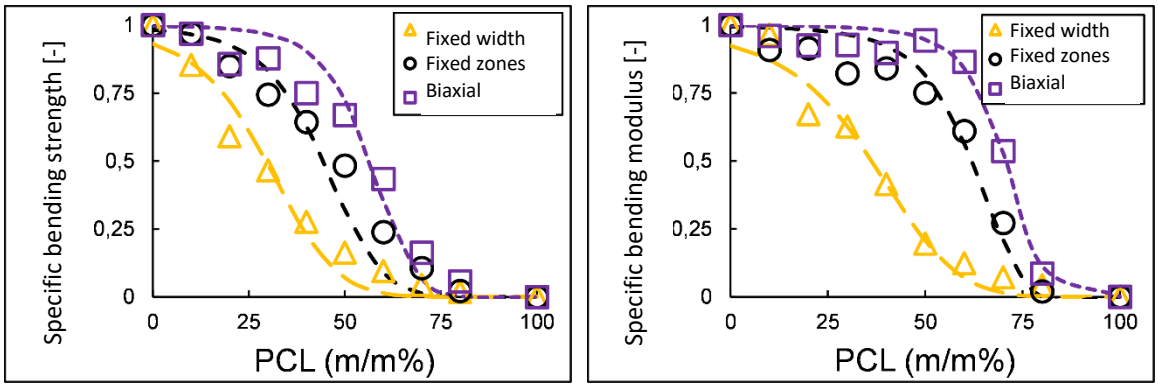

Figure 22. Fitting of the Hill equation on the specific three-point bending test results

Parameter	Specific bending strength			Specific bending modulus		
	Fixed width	*Fixed zones*	*Biaxial*	*Fixed width*	*Fixed zones*	*Biaxial*
A	1	1	1	1	1	1
n	7,48	7,28	7,32	5,49	5,43	5,36
$K_{0,5}$	70,52	55,66	43,58	63,79	38,19	29,38

Table 2. Hill equation parameters of the curves fitted to the bending test results

Looking at the parameters of the equation, it can be observed that the exponent values show small deviations within the strength and modulus values and can be considered as reaction constants within given groups. The value of K0.5, however, shows a decreasing trend for both strength and modulus values, i.e., the values start to decrease later as the distance between the samples increases.

In the tensile tests (Zwick Z020, 5 mm/min, 80 mm gripping distance) we used DIC (digital image correlation) strain measurement (device: Mercury Monet), and we collected acoustic data using Acoustic Emission (AE) (microphones: Physical Acoustic Corporation Micros30s, AE device: Sensophone AEPC-40/4).

Figure 23 shows the expected crack propagation mechanism. Firstly, the crack propagates through the EP matrix material and then reaches the CF reinforcement fibers (Figure 23; a). The reinforcement fiber breaks under load, causing excessive stress in the area around the reinforcement fiber, leading to rapid crack propagation and further fiber breaks in case of the unmodified composite (Figure 23; b). The role of the modified zones is to slow down the reinforcement fiber breakage and the rapid propagation of the crack, here it can be seen that the crack reaches the modified zone, and localized damage occurs (Figure 23; c). This allows the material to absorb more energy and in the case of excessive loading, the failure is not instantaneous. The results are presented in Figure 24.

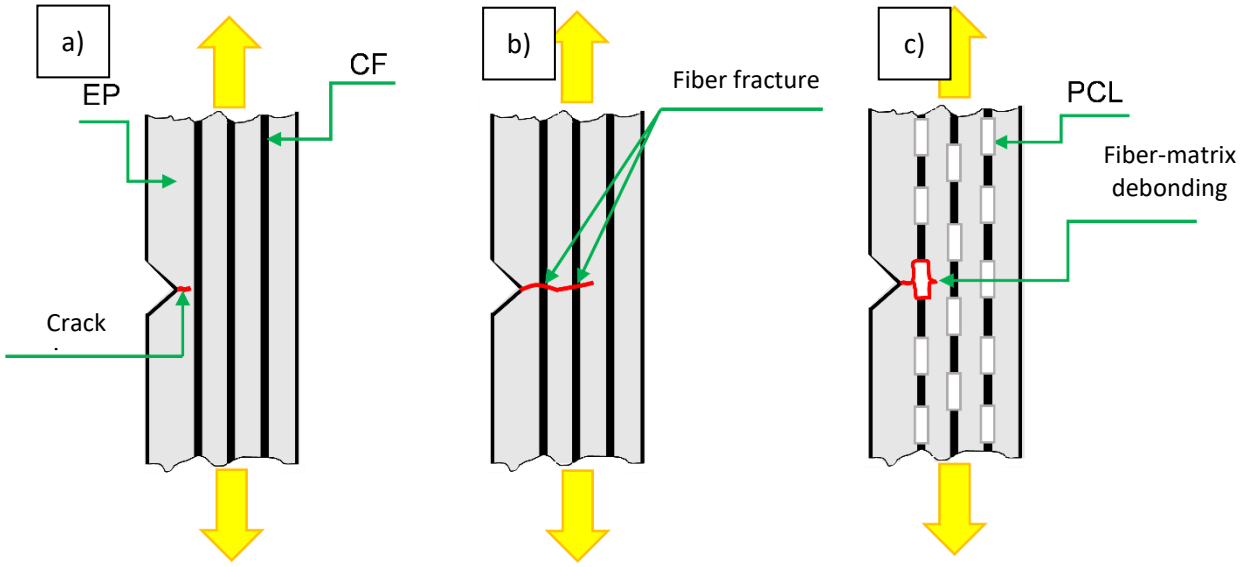

Figure 23. Assumed failure mechanism in an unmodified (b) and modified interface composite (c) in tensile setup

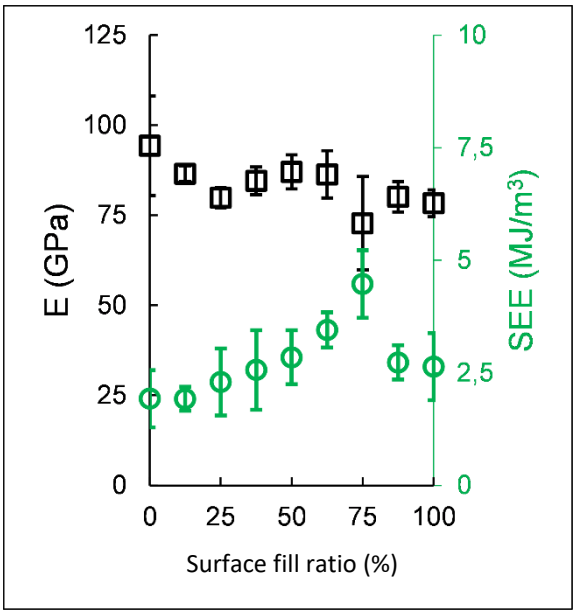

Figure 24. Young's modulus and specific absorbed energy measured in the tensile tests

Acoustic emission measurements can be used to gain a deeper understanding of the nature of the processes involved in the failure process. From the cumulative event counts (Figure 25), it can be inferred that the reference samples exhibited a more brittle type of failure, based on the proportionally higher number of signals in the higher amplitude range (>60 dB). For these samples, the typical damage pattern was fiber fracture. However, for the modified samples, a higher amount of signals was observed at lower amplitude events (34-40 dB), representing interface damage. This suggests damage with lower energy release, which in this case represents local damage. Due to the local interface modification, the dominant damage pattern was no longer fiber fracture in the modified samples. This also supports the previous findings in the thermocamera images in Figure 9.

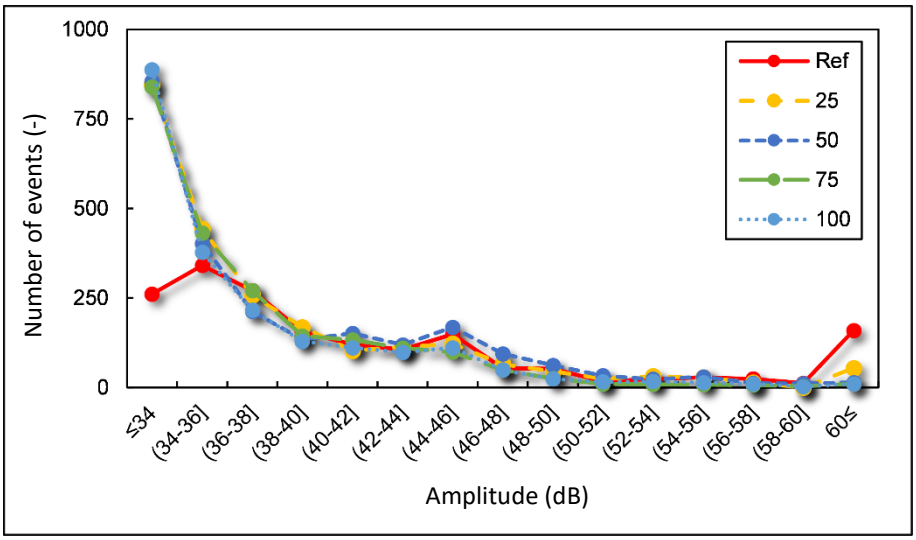

Figure 25. AE amplitude histogram of the tensile tests (numbers in the legend represent surface fill ratio in %)

To get insight into the dynamic properties and mechanisms, instrumented Charpy impact tests were performed (Ceast Resil Impactor Junior, DAS 8000 data acquisition system, 15 J impact energy, 3.7 m/s impact speed) with flatwise impact. The results are presented in Figure 26.

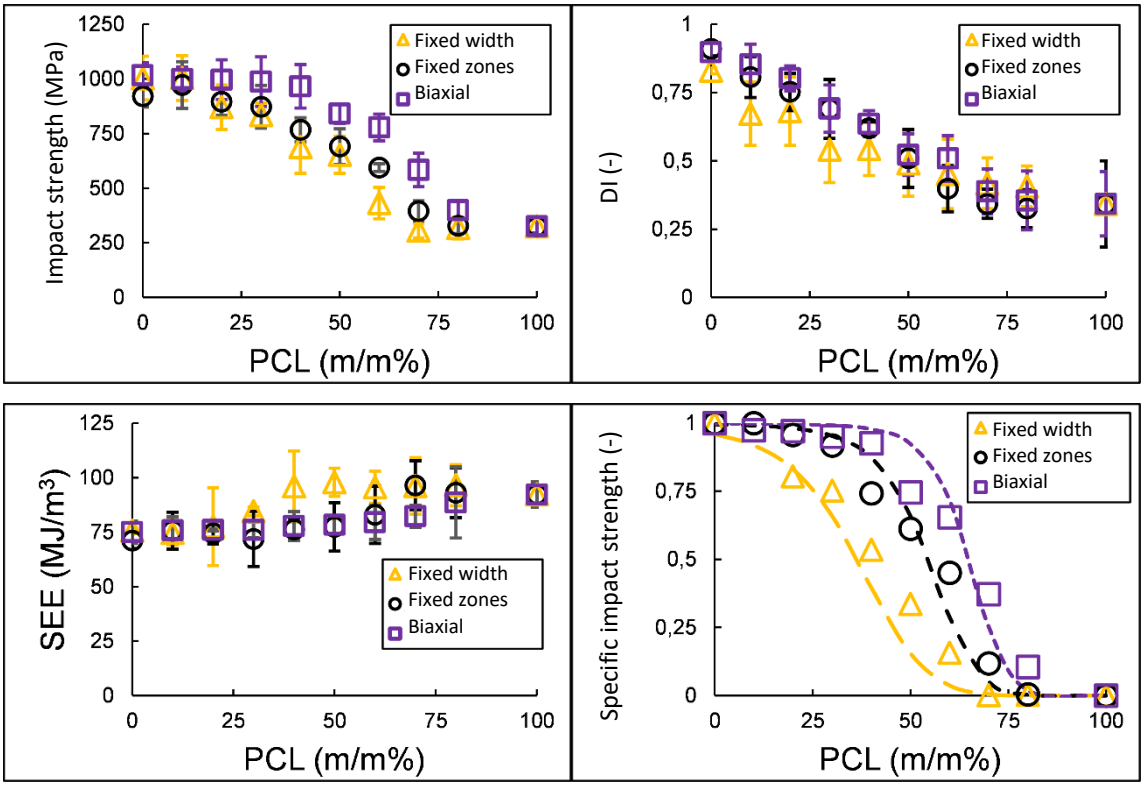

Figure 26. Results of the instrumented Charpy impact tests

The evaluated values gave similar results to the static tests, the impact strength decreased when reaching approximately 40% PCL content, while the ductility (DI decrease) and the specific absorbed energy (SEE) were constantly improving. Similarly to the three-point bending tests, a Hill model was fitted to the specific impact strength measured points, which gives us information about the failure process (Figure 26, bottom right).

To gain further insight into the crack propagation modification provided by the interlaminar patterns, ENF (end-notched flexure) tests were performed. Here in the middle layer, containing the precrack (provided by a PTFE film), diagonal biaxial patterns were printed. The surface filling was set in 12.5% steps up to 100%. The layout is presented in Figure 27.

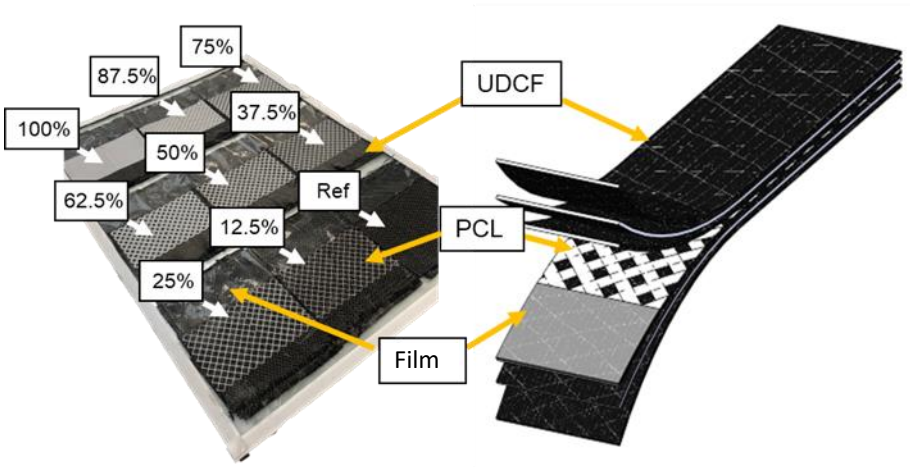

Figure 27. The layout of the specimens used for the ENF tests

The bending stress-strain curves show that the presence of PCL in the specimens reduces the value of the first stress peak in the composites. The specimen with the lowest PCL content (12.5%) showed the largest decrease, and as the PCL content increased, the stress values started to increase and approached the value obtained in the reference specimen. These stress peaks appear at increasingly higher deformation values as the PCL ratio increases. The increase in the deformation values is due to the presence of PCL, where the crack meets the locally modified printed zone where the crack propagation rate slows down, thus not propagating explosively as in the reference samples. As the surface fill ratio increases, the first and second stress peaks begin to merge, with distinct peaks appearing at low ratios, but a plateau develops for samples with higher PCL ratios, where crack propagation shows a gradual character (Figure 28).

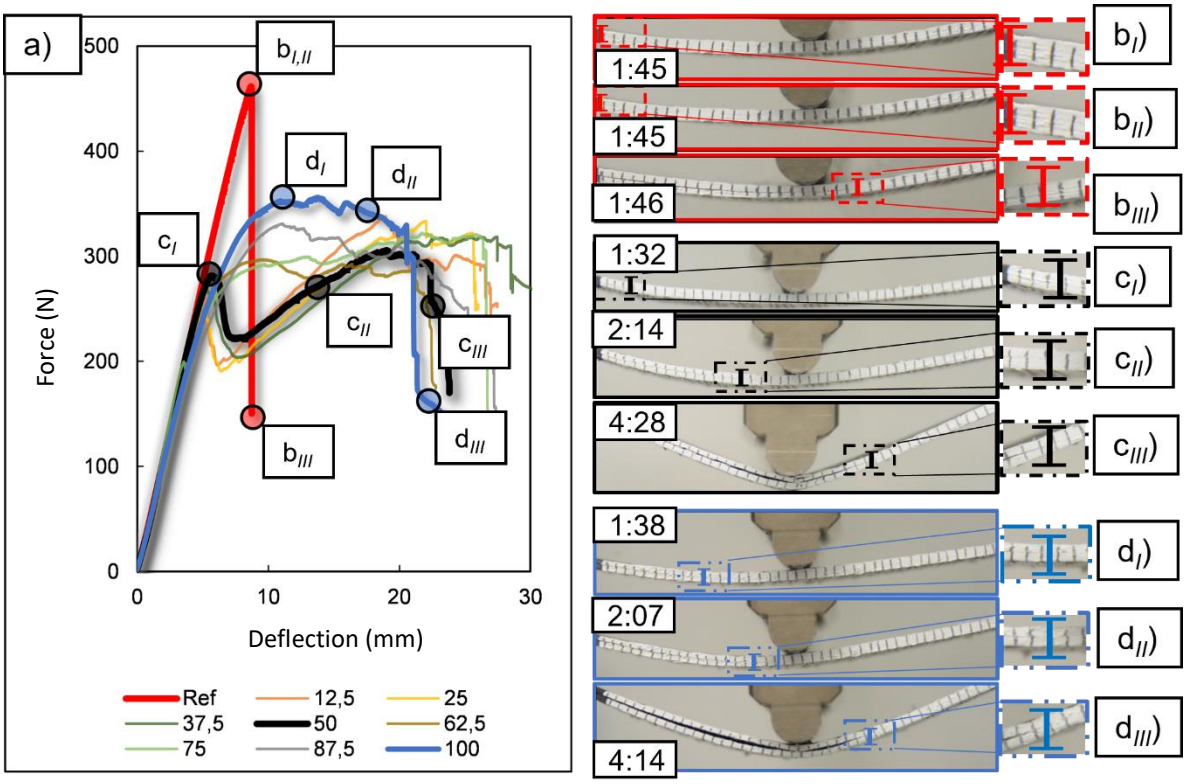

Figure 28. Typical curves of the ENF tests (a) and characteristic failure progress (b-d)

From the evaluation of the critical stress concentration factors (G_{IIC}) presented in Figure 29, it can be seen that as the PCL ratio increased, the value of the stress intensity factor increased. Compared to the reference values, an increase of up to 50 % was achieved for composites with a high PCL ratio. This increase can be explained by the force-deflection and stress-deformation diagrams, as the first stress peaks appeared at higher deflection values, while the maximum force did not decrease as much.

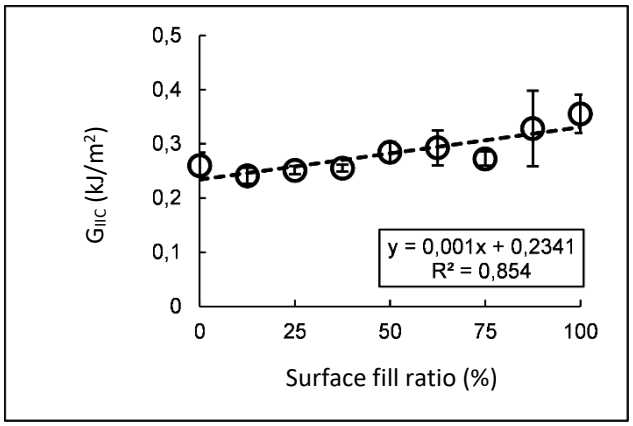

Figure 29. Evaluated critical stress concentration factors (G_{IIC}) from the ENF tests

In addition to the critical stress intensity factor, which only gives information about the energy required for crack propagation initiation (at one point), more information is given by the so-called resistance curve (R-curve, Figure 30). The resistance curves can be used to determine the energy required for crack propagation at a given moment in time. This allows the crack propagation energy for the whole damage to be determined.

For the reference specimens, the failure exhibits a brittle behavior, i.e. no further resistance occurs after reaching the G_{IIC}, and no further crack propagation has occurred. However, with the PCL layer, a more stable type of propagation appeared. No final failure occurred at the onset of the first crack propagation. This is due to local blocking of the delamination. In the reference sample, the initial failure propagated between the layers immediately after reaching G_{IIC}, causing brittle failure. With PCL, more energy was required for the layer separations to occur, in several cases, the defect did not appear in the fault plane but propagated to another layer. As a result, a more ductile type of failure occurred.

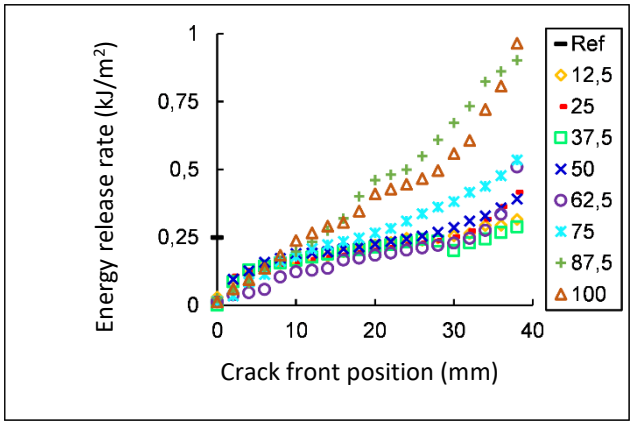

Figure 30. R-curves of the ENF tests

4. Investigation of healing properties

The inclusion of a thermoplastic interlaminar pattern in the composites opens the possibility of healing the composite by applying heat and pressure. In the healing process, the thermoplastic polymer melts and can fill the cracks or at least blunt the crack tips formed in the structure. Our aim in the present research was to demonstrate the healing effectiveness and provide some guidelines for optimal parameter selection.

The healing was performed on ENF specimens tested with the same parameters as before but with limited damage. The healing was performed in a Collin Teach-Line Platen Press 200E hydraulic press. Specimens with 25, 40, 55, 70, 85, and 100% surface fill were tested. For each test, the healing efficiency, calculated from the measured healed value divided by the initial value was used to characterize the process. In the curves, a saturation process could be identified with the increasing surface area fill. To gain further insight into the processes, a model, composed of a dead-lag and a proportional element was fitted to the results. Besides the surface fill ratio, the pressure, and the healing time was changed to investigate the effect. The heal temperature was set to 65°C, above the melting temperature of the PCL and below the Tg of the epoxy resin. The obtained curve sets are presented in Figure 31 and 32.

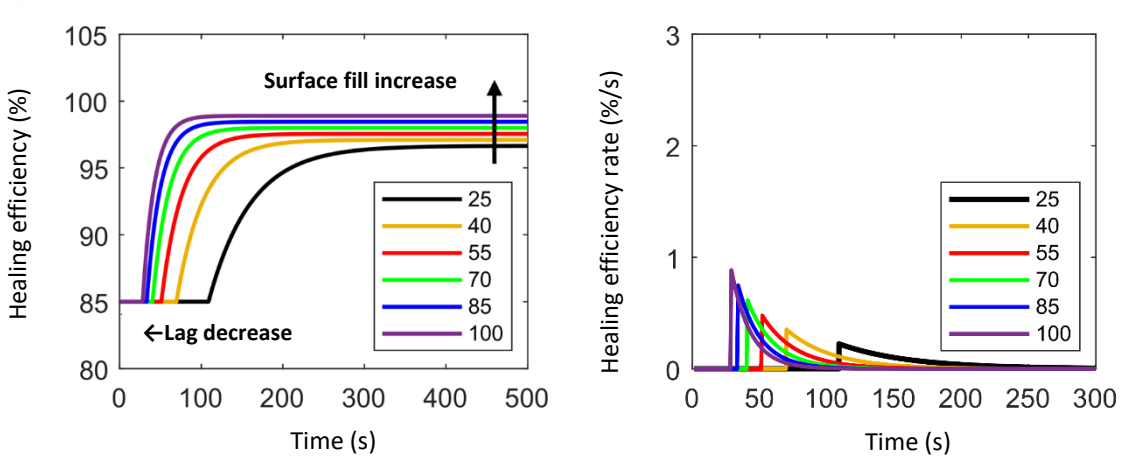

Figure 31. Curves obtained at fixed 1 bar healing pressure

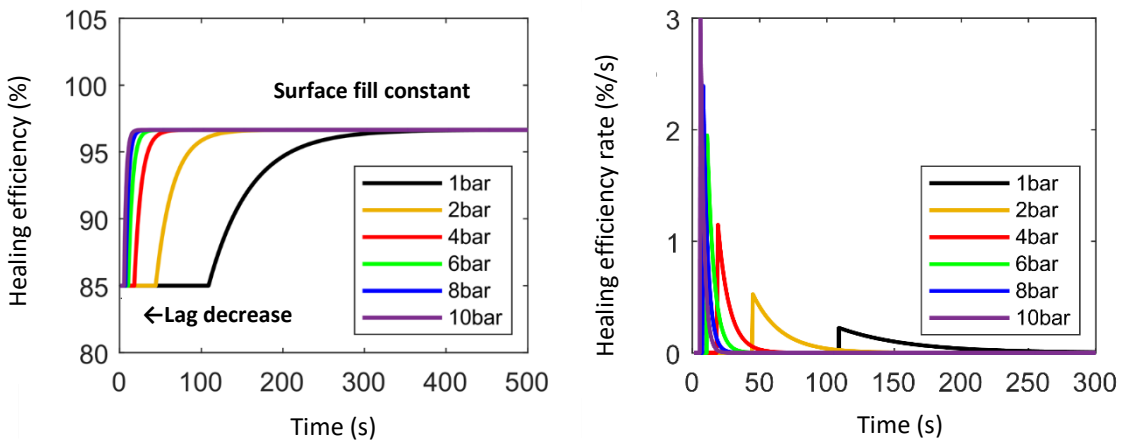

Figure 32. Curves obtained at fixed 25% surface fill ratio

From the preliminary results, the parameters used in the fitting showed pressure and concentration-dependent properties (τ, Th). This is due to the fact that during the process, pressure accelerates the reaction rate. At higher pressures, the cracks formed are filled faster. Furthermore, the concentration has a similar effect on the two previous factors, with higher filling levels resulting in faster filling of the cracks due to the excess material. For the proportional member, only a concentration dependence is observed. This is because the maximum cure efficiency that can be achieved depends only on the PCL present in the system, with pressure only affecting the reaction rate. The functions fitted to the results are described by equations (2-4).

$$\tau_{(c,p)} = \alpha c^{-\beta} p^{-\gamma} \quad (2)$$

$$A_{(c)} = -\delta \cdot c + \varepsilon \quad (3)$$

$$T_{h_{(c,p)}} = ln\left(1 - \frac{H_0}{A_{(c)}}\right) \cdot \tau_{(c,p)} \quad (4)$$

where "τ(c,p)" is the time constant, which is concentration and pressure-dependent, "A(c)" is the proportional term, which is concentration-dependent, "Th(c,p)" is the dead time, which is concentration and pressure-dependent, and "H0" is the efficiency of curing uncured composites (H0=85). The value of the proportional term depends only on the concentration. The behavior shown follows a linear character, so we have incorporated this into the model (Figure 31-32). Furthermore, from the derivative function, it is observed that the reaction rate is also affected by the concentration. As the concentration increases, the healing process is accelerated, and the derivative (rate) reaches the value 0 sooner, i.e. the maximum healing for a given concentration level can be reached sooner. This is also true for the dead-time term, which shows a continuous, exponential decrease in the curves describing the healing process. The models were validated by the testing of the next set of samples, produced with 37.5, 62.5, and 87.5% surface fill ratio patterns. The measured points with the previously fitted model results are presented in Figure 33. The model showed a very good prediction. It can be further used for process optimization of healing of the interlaminar patterned composites.

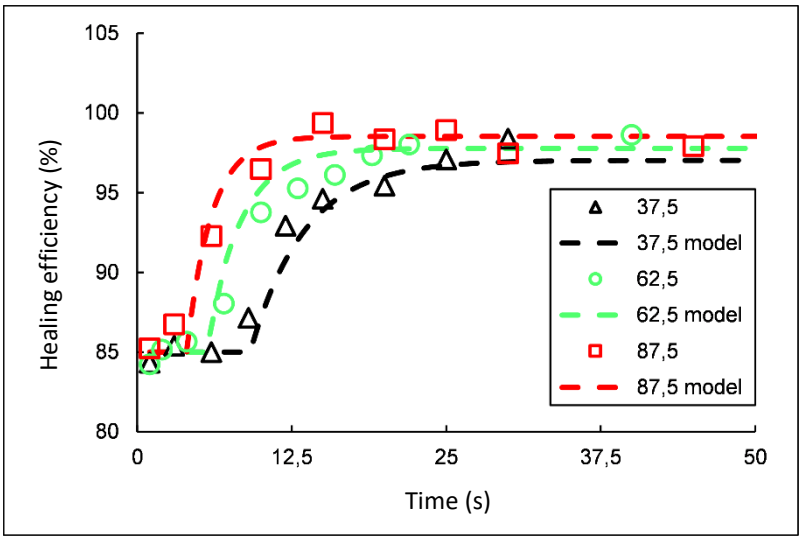

Figure 33. Validation of the model with test results

Finally, the possibility of several healing cycles was investigated by retesting and rehealing of the composites in several (up to 12) healing cycles with the optimized pressure and dwell times. The results of the test series are presented in Figure 34.

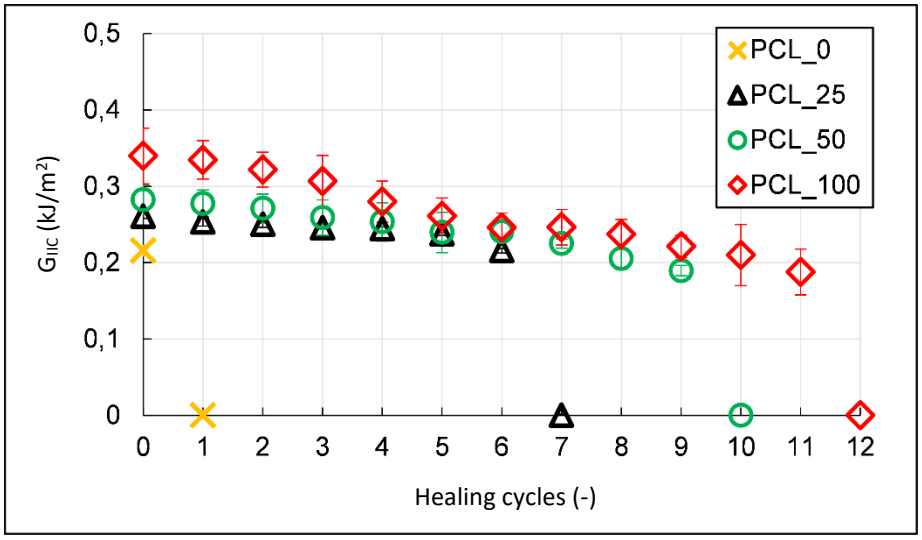

Figure 34. Effect of repeated healing cycles on the critical stress concentration factors (G_{IIC})

By increasing the concentration of interlayer material, the composite was able to withstand significantly more cycles. This is because the excess material was able to fill the cracks that occurred during the cycles over more cycles. There was more material available. This resulted in higher critical stress concentration values, similar to previous measurements.

The healing of three-point bent fractured specimens were also investigated. Here also, the optimized healing parameters were used. The results are presented in Figure 35.

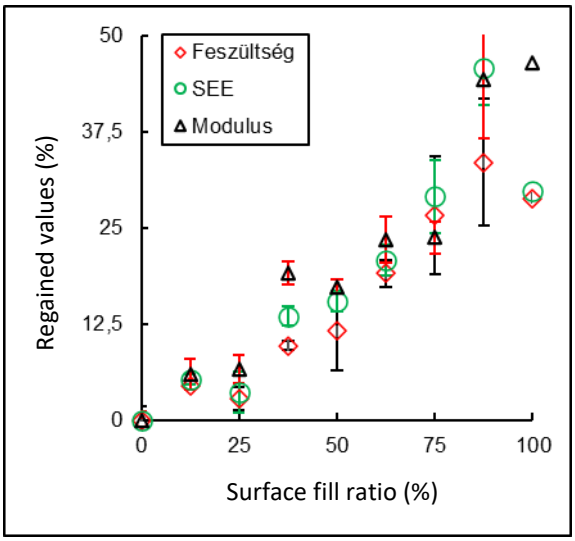

Figure 35. Regained values of healed, previously broken three-point bent specimens

The results show, that the healing is effective not only in fracture mechanical specimens, but also in globally fractured specimens, so it can be used in real-life situations for temporary repair.

5. Summary

The aim of the project was to develop technologies for ductility improvement of composites via interfacial engineering. Three different technologies were developed and proved to be effective. The mechanisms of the failure changing effect of the interlaminar patterns were investigated in classical static and dynamic tests, as well as fracture-mechanical investigations. The application of modeling helped to gain further insight into the processes. The possibility of healing was also investigated and demonstrated, and a model was created, which can be used for healing optimization and which can be adapted to other healing technologies.

Besides the main goals, several subtopics were introduced, and new results were achieved in the field of damage monitoring and characterization in composites (by digital image correlation and embedded fiber Bragg grating (FBG) sensors), using electrospun interlayers for damage modification and creation of novel simulation tools for composites. These results are available in the publications of the project.

Generally, we can declare that the project was successful and the goals have been achieved. The results can be industrially applied and can also serve as a basis and starting point for further research.

6. Dissemination

The results of the project were published in scientific journals and conferences at the international level. The main achievements for the project duration are summarized below:

Number of conference proceedings: 14

Number of scientific articles: 9

Number of scientific articles with impact factor: 7

Total impact factor: 36.474

The researchers were able to present the results at International ICCST12 Conference on Composite Science and Technology in Sorrento (Italy), ICCM22 in Melbourne (Australia) in 2019, and at ECCM20 in Lausanne (Switzerland) in 2022. All presentations received positive feedback. Two D1 IF publications were prepared. Five more IF articles (Q1 and Q2) are prepared and submitted from the results at the time of reporting.

In connection with the projects, two PhD students have prepared their theses, and both are submitted for the internal defense at the time of the writing of the report:

Balázs Magyar – Development of polymer composites with designed interfacial adhesion (Supervisor: Dr. Gábor Szebényi)

Viktor Hliva – Non-destructive characterization of composite structures using digital image correlation (Supervisor: Dr. Gábor Szebényi)

Our aim was to involve also university students in the project. The following number of theses and student scientific works were created on the topic of the project:

BSc theses: 5

MSc theses: 12

Student's Scientific Committee presentations: 2